Angewandte Zuschriften

Isomerization

Deutsche Ausgabe: DOI: 10.1002/ange.201411894
Internationale Ausgabe: DOI: 10.1002/anie.201411894

# Direct Measurement of the Isomerization Barrier of the Isolated Retinal Chromophore**

*Jonathan Dilger, Lihi Musbat, Mordechai Sheves, Anastasia V. Bochenkova, David E. Clemmer, and Yoni Toker**

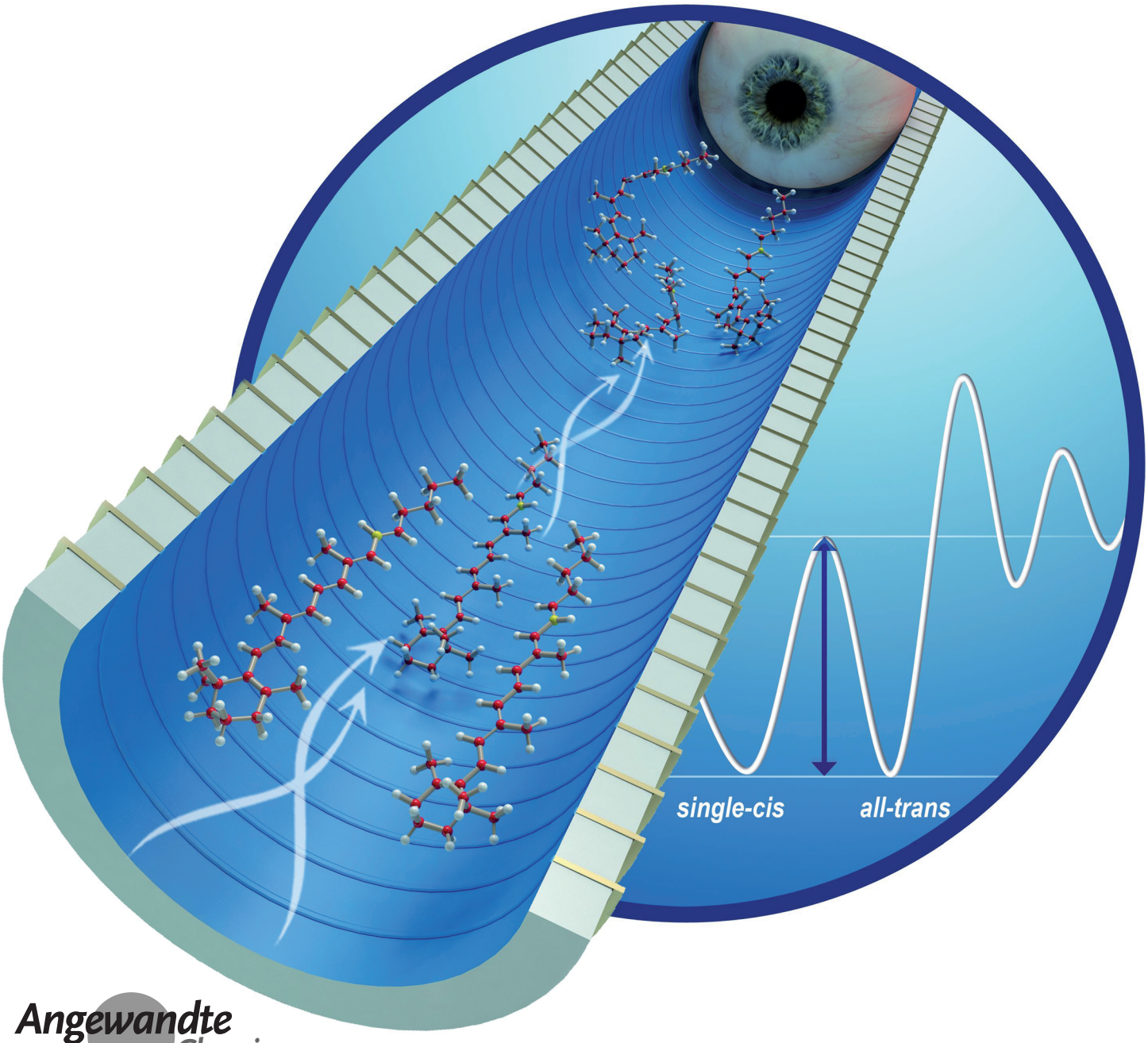


Angewandte Chemie

***Abstract:*** *Isomerizations of the retinal chromophore were investigated using the IMS-IMS technique. Four different structural features of the chromophore were observed, isolated, excited collisionally, and the resulting isomer and fragment distributions were measured. By establishing the threshold activation voltages for isomerization for each of the reaction pathways, and by measuring the threshold activation voltage for fragmentation, the relative energies of the isomers as well as the energy barriers for isomerization were determined. The energy barrier for a single cis–trans isomerization is (0.64 ± 0.05) eV, which is significantly lower than that observed for the reaction within opsin proteins.*

The retinal protonated Schiff-base (RPSB) chromophore, illustrated in Figure 1, is the optical switch which plays a key role in the vision of animals, and is also used for phototropism in bacteria and proton pumping in *archae*.[1–4] In vision the chromophore is found in the center of rhodopsin, a protein embedded in the membrane of rod and cone cells in the retina of the eye. Upon absorption of a photon the chromophore undergoes a photoisomerization which triggers the surrounding protein. Protein conformational alterations eventually lead to the closing of an ion channel and to the production of an electrical signal. Sheves et al. have suggested[5] that the height of the isomerization barriers is key to understanding the difference in isomerization pathways between rhodopsins and bacteriorhodopsin. The properties of the chromophore, such as its maximal absorption wavelength, $\lambda_{max}$, the barrier energy for isomerization, $E_a$, and isomerization efficiency, can be tuned by the surrounding protein. Indeed, different rhodopsin proteins absorb light at different wavelengths, which is key to color vision. By measuring the rate of "dark counts" as a function of temperature, the Arrhenius activation energy have been measured to be in the range of 23 to 27 kcal mole$^{-1}$ (corresponding to 1–1.2 eV) and found to scale linearly with $1/\lambda_{max}$.[6] This finding, known as the Barlow correlations, is still not fully understood despite extensive studies.[7–10] In particular, the energy barrier on the potential energy surface may be different from the Arrhenius activation energy, and has been estimated to be up to 50 kcal mole$^{-1}$ (ca. 2 eV).[8] Herein we show that the intrinsic barrier for isomerization of the isolated molecule is below the value found when bound inside rhodopsin. Thus we propose that rhodopsin restricts isomerization and thus regulates photon signals.

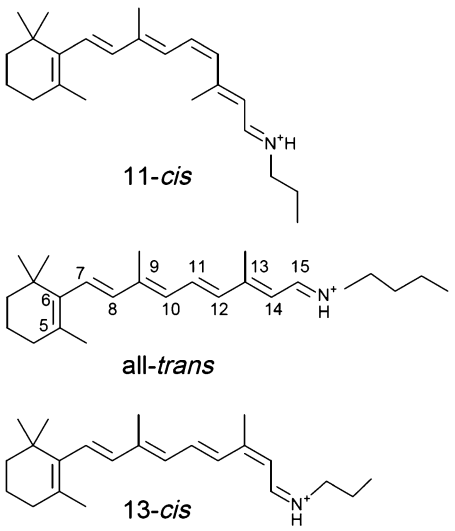


***Figure 1.*** Structure of several of the important isomers of the RPSB. In vision photoabsroption leads to a transition from the 11-*cis* to the all-*trans* isomer. In *archae* photoisomerization is from the all-*trans* to the 13-*cis*.[1–4]

In understanding the mechanisms by which the protein tunes the properties of the chromophore, it is beneficial to perform gas-phase measurements in which the properties of isolated chromophores are measured. Indeed, gas-phase measurements have proven to be instrumental in understanding the color-tuning mechanism of the protein.[11] The first ion mobility spectrometry (IMS) measurements of the RPSB were performed recently by Bieske et al.[12,13] IMS allows the differentiation between conformations of a given isolated molecular ion by dragging the ions through a drift tube filled with a buffer gas with an electric field. By measuring the drift time of the ions one can determine their collisional cross-section and in the case of multiple isomers one can measure the isomer distribution. Bieske et al. observed four structural peaks in the IMS spectrum of the RPSB. They proceeded to irradiate the chromophores using a tunable laser prior to the drift tube and measured the change in mobility as a function of the laser wavelength. Measuring isomerization of isolated molecular ions has recently become possible using a technique known as IMS-IMS-MS.[14] Moreover, it has been shown that this technique can be used to measure fragmentation energies and internal energy barriers.[15–17] IMS-IMS uses two drift tubes with an activation region in between. The first drift tube is used for isomer separation and mobility-selected ions are then excited in the activation region (via energetic buffer gas collisions), and the resulting distribution of isomers is measured using the

[*] Dr. J. Dilger
Spectrum Warfare Systems Department, NSWC Crane Division
Crane, IN 47522 (USA)
L. Musbat, Dr. Y. Toker
Institute of Nanotechnology and Advanced Materials, Bar-Ilan University, Ramat-Gan 290002 (Israel)
E-mail: yonitoker@gmail.com
Prof. M. Sheves
Chemistry Department, Weizmann Institute of Science
Rehovot 978007 (Israel)
Dr. A. V. Bochenkova
Department of Physics and Astronomy, Aarhus University
DK-8000 Aarhus C (Denmark)
Dr. A. V. Bochenkova
Department of Chemistry, Moscow State University
119991 Moscow (Russia)
Prof. D. E. Clemmer
Department of Chemistry, Indiana University
Bloomington, Indiana 47405 (USA)

[**] We would like the thank Matthew Glover, Steen Brøndsted Nielsen, and Nicholas Pierson for their help and valuable advice on this project.

  

second drift tube. In this work we use IMS-IMS to measure the energy barriers for isomerizations of the RPSB.

The experiments were conducted in the two-meter IMS-IMS-MS system which was described in detail previously.[14–17] The system consists of two successive one-meter-long drift tubes followed by a time-of-flight mass spectrometer. Ions produced by nanospray are accumulated before the entrance of the first drift tube and then pulsed into the drift tube at a rate of 10 Hz. Within the drift tube, helium buffer gas is maintained at a pressure of 3 Torr, and a constant electric field of $E = 9.7\ \mathrm{V\,cm^{-1}}$ is applied. The activation region lying in between the two drift tubes consists of two electric grids. By pulsing the voltage on the first grid one can allow only ions of a specific mobility to pass. By applying an activation voltage, $V_{act}$, between the two grids, the ions are collisionally activated, which causes them to isomerize. The second drift tube is used to measure the resulting distribution of isomers. These measurements will be referred to as "selection and activation" measurements. At the exit of the second drift tube the ions are pulsed into a time-of-flight mass-spectrometer. The millisecond timescale of the mobility separation coupled to the microsecond timescale of the mass analysis allows these datasets to be collected in a nested fashion. It is useful to convert the drift-time distribution to cross-section distributions by using the following relation:

$$\Omega = \frac{\sqrt{18\pi}}{16}\frac{ze}{\sqrt{k_B T\mu}}\frac{t_D E_{dc}}{L}\left(\frac{760}{P}\right)\left(\frac{T}{273.2}\right)\frac{1}{N} \qquad (1)$$

Here $ze$ is the ion's charge, $k_B$ is the Bolzmann constant, $L$ is the length of the drift tube, $\mu$ is the reduced mass of the ions and buffer gas molecules, $T$ is the temperature, and $N$ is the neutral number density at standard temperature and pressure. Figure 2 shows the cross-section distribution recorded for the RPSB chromophore (mass 340 amu). The cross-section distribution of the RPSB consists of two prominent close-by peaks, labeled A and B, whose collisional cross-section corresponds to 150 and 148.5 Å$^2$ respectively. Around 5% of the population lie within a third peak, labeled X, with a cross-section of 138 Å$^2$. A tiny additional feature, labeled Y, appears at a cross-section of 143.5 Å$^2$. The IMS measured by Bieske et al.[12] is similar in that it consists of four peaks, two of which have dominant, large cross-sections. The cross-sections recorded here for the two peaks are a little less than 30% of the values reported by Bieske et al., consistent with cross-section differences commonly observed when using instruments having $N_2$ as the buffer gas. Nevertheless, the population and positions of the two smaller peaks are different, and therefore they are labeled differently here (X and Y instead of C and D). The all-*trans* isomer has the largest collisional cross-section, with a calculated collisional cross-section[18,19] which agrees within 5% with the measured position of peak A. The calculated cross-sections of the 9-*cis*, 11-*cis*, and 13-*cis* isomers are 3% lower than that of the all-*trans* isomer, and they all fall within the range of peak B. As such we have assigned peak B to correspond to multiple isomeric geometries which likely contain a single *cis* isomerization. Peaks X and Y correspond to isomers with multiple *cis* bonds, and perhaps also cyclized isomers, such as those seen in Figure 3. These isomers are not relevant for the dynamics within the protein, however they play a role in the gas-phase fragmentation of the RPSB. Using MS-MS we have recently shown[20] that the RPSB fragmentation process involves a series of isomerizations and a Diels–Alder cyclization, and the eventual emission of a toluene molecule. The mechanism we suggested involves the formation of a three-ring structure shown in Figure 3a. Based on ion mobility measurements of the photofragments, Bieske et al.[21] have shown that cyclization does indeed occur, however, through a different mechanism involving the formation of the intermediary structures shown in Figure 3b and c.

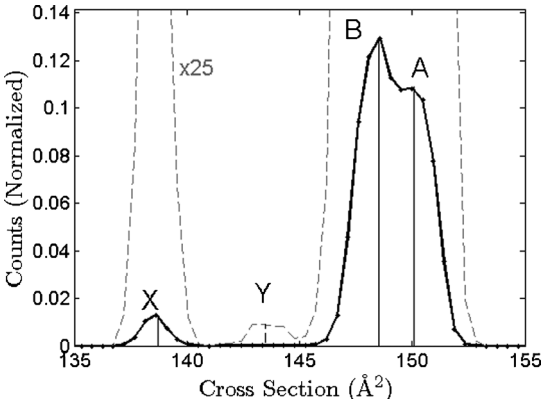


***Figure 2.*** IMS of the RPSB. The dashed line corresponds to the same spectrum magnified times 25. Four structural peaks are apparent and are labeled here as A, B, X, and Y.

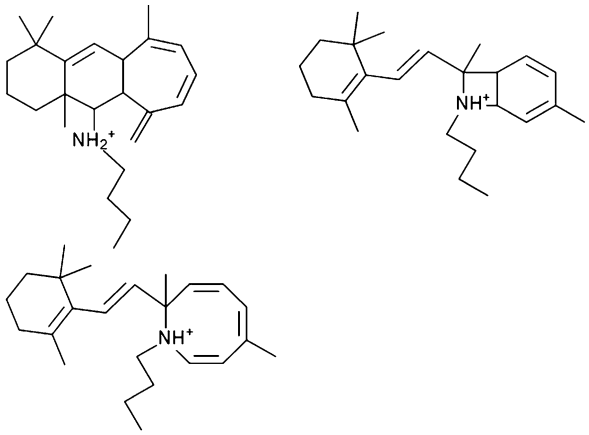


***Figure 3.*** Structure of several compact isomers of the RPSB

Figures 4 and 5 present the results from two of the selection and activation scans, where the selection was applied to peaks A and Y, respectively. In these measurements the activation voltage was scanned in steps of 10 V up to 200 V. Selection and activation scans were also performed on peaks B and X. When selection is applied to peak A one does not see a change in isomer distribution for $V_{act} < 70$ V. Above $V_{act} = 70$ V peak B begins to form, and at $V_{act} > 100$ V additional features associated with X appear at lower cross-sections. The threshold fragmentation voltage is $V_{act} = 110$ V.

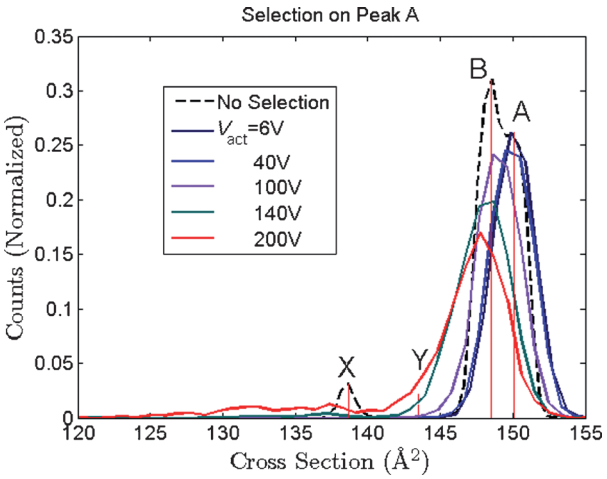


***Figure 4.*** Results of selection and activation when the selection is applied to peak A, and activation is performed for different activation voltages, $V_{act}$. The dashed line corresponds to the IMS of the RPSB with no selection.

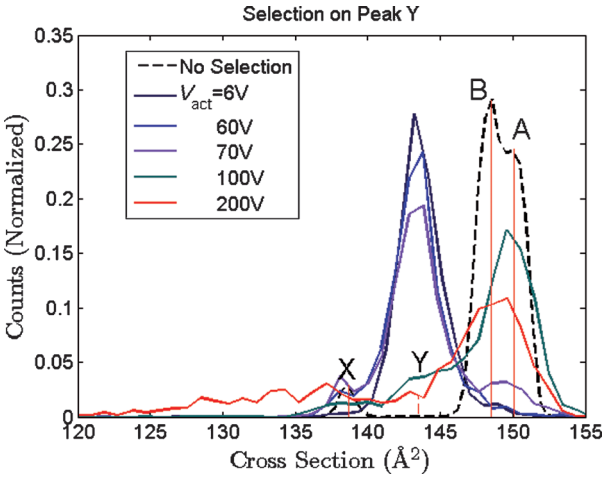


***Figure 5.*** Results of a selection and activation scan, where selection is applied to peak Y.

The thresholds for isomerizations starting from peak Y are lower: 50 V for isomerization into X and 60 V for isomerization into peaks A and B. By summing the counts in the regions associated with the different peaks as a function of $V_{act}$ we arrive at threshold plots such as those shown in Figure 6. Similar to previous works[15–17] we define the threshold activation voltage as the voltage where a change in relative intensity of 1 % is observed. In the case of selection on peak A the threshold activation voltage for isomerization into B is found to be $V_{A\text{-}E} = 70$ V. Interestingly in the case of selection on peak B, the population of peak X steadily increases until $V_{act} = 70$ V at which point it decreases again, until $V_{act} = 110$ V, when the population of X begins to grow again. From similar plots derived from the different selection and activation scans, we deduced the threshold activation voltage for the various isomerizations as well as the threshold activation voltage for fragmentation. Recently, it has been shown semi-empirically[11] that the activation voltages divided by the number of

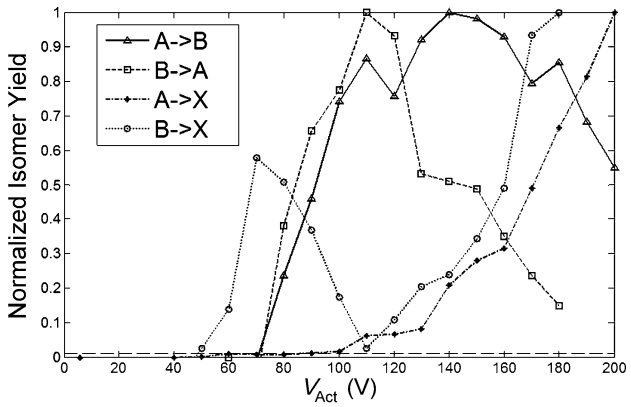


***Figure 6.*** Thresholds plot used to derive the activation voltage for each transition. A plot of $\alpha \rightarrow \beta$ shows the abundance of structural feature $\beta$ when selection is applied on feature $\alpha$ normalized by the maximum abundance reached. The dashed black line indicates a relative abundance of 1 %.

degrees of freedom of the molecule scale linearly with the barrier energies. Thus one can translate the threshold activation voltages into energy barriers.[16,17] The present work was conducted on the same apparatus, with the same conditions, such that the calibration of activation voltage to barrier height could be used. We assume that the linear dependence between the normalized activation voltages and barrier heights holds true in a wide range of energies for systems similar in size to those used to construct the calibration curve and there are no dramatic corrections to the correlation because of the entropically related differences between reactions studied here and those used for the calibration.[16,17] The results are summarized in Table 1.

The energetic story which is told by this data is illustrated in Figure 7. From the barrier energies for fragmentation we can determine the relative energies of the different structures. Interestingly, the barrier energy for isomerization from structure B into X is significantly smaller than the barrier for A→X. Moreover the energy barrier for isomerization is smaller than the potential energy of structure X. From this data we conclude that there exist at least two structures with similar mobilities, and we label them X and X*. At an

***Table 1:*** Energy barriers for isomerization and fragmentation measured in this work.

| Process | $V_{act}$ | Barrier energy [eV] |
|---|---|---|
| A→X | 90 | 0.8 ± 0.05 |
| B→X | 40 | 0.4 ± 0.05 |
| Y→A | 60 | 0.56 ± 0.05 |
| Y→B | 60 | 0.56 ± 0.05 |
| Y→X | 50 | 0.5 ± 0.05 |
| X→A | 50 | 0.5 ± 0.05 |
| X→B | 50 | 0.5 ± 0.05 |
| A→B | 70 | 0.64 ± 0.05 |
| B→A | 70 | 0.64 ± 0.05 |
| A→frag | 110 | 1 ± 0.05 |
| B→frag | 110 | 1 ± 0.05 |
| Y→frag | 50 | 0.5 ± 0.05 |
| X→frag | 40 | 0.4 ± 0.05 |

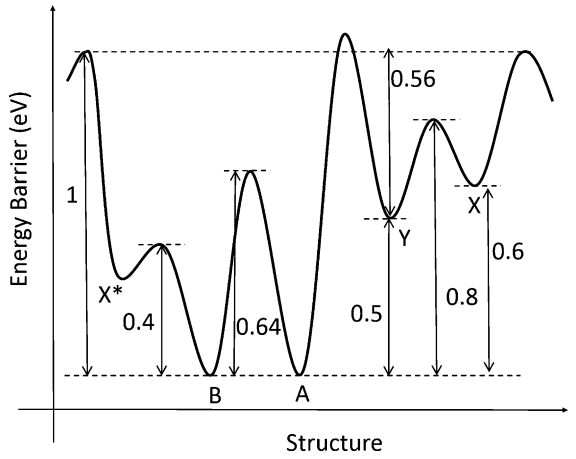


***Figure 7.*** Schematic illustration of the energy diagram of the RPSB. The ground-state energies and energy barriers for isomerizations of the different structures studied here are shown.

activation voltage of 40 V structure B isomerizes into X*. At $V_{act} = 70$ V structure B begins to isomerize into structure A, and causes a decrease in the population of structure X*. This proccess explains the initial rise and subsequent fall of the B→X curve shown in Figure 5. The rise of the curve starting at $V_{act} = 110$ V probably corresponds to isomerization into structure X. Interestingly the structure X* is not accessible when starting from structure A. Notably, the threshold for fragmentation is only slightly larger than that of isomerizing into structure X*. This observation agrees with the proposed gas-phase fragmentation mechanisms[14,15] which involves the formation of a compact intermediary structures prior to fragmentation.

The most important observation in this work is that the energy barrier for a single *cis–trans* isomerization (the energy barrier for the A→B and B→A transitions) is (0.64 ± 0.05) eV. This value is significantly lower than expected barrier heights for thermal isomerization of double bonds. Nevertheless it should be noted that the ground electronic state of the RPSB is a superposition of several resonance structures where the positive charge is delocalized along the polyene chain and located mostly on either C5, C9, C13, or the protonated Schiff-base linkage (the last resonance structure is the one depicted in Figure 1), with a corresponding rearrangement of the molecular bonds. Thus the character of the molecular bonds along the conjugated chain is in between that of a single and a double bond. The measured energy barrier is also significantly lower than the energy barriers measured within the rhodopsin protein (1–2 eV range). Thus the protein has a significant role in increasing the barrier energy for thermal isomerization relative to that in the gas phase, wherein interaction with the RPSB counterion and steric constraints are lacking. A high barrier energy is mandatory for efficient vision processes, otherwise thermal noise would overwhelm the signal originating from the photochemical isomerization.

**Keywords:** chromophores · gas-phase reactions · ion mobility spectroscopy · isomerization · proteins

**How to cite:** *Angew. Chem. Int. Ed.* **2015**, *54*, 4748–4752
*Angew. Chem.* **2015**, *127*, 4830–4834

[1] R. R. Birge, *Biochim. Biophys. Acta Bioenerg.* **1990**, *1016*, 293–327.
[2] R. S. Becker, *Photochem. Photobiol.* **1998**, *48*, 369–399.
[3] J. L. Spudich, C. S. Yang, K. H. Jung, E. N. Spudich, *Annu. Rev. Cell Dev. Biol.* **2000**, *16*, 365–392.
[4] O. P. Ernst, D. T. Lodowski, M. Elstner, P. Hegemann, L. S. Brown, H. Kandori, *Chem. Rev.* **2014**, *114*, 126–163.
[5] M. Sheves, T. Baasov, *J. Am. Chem. Soc.* **1984**, *106*, 6840–6841.
[6] R. B. Barlow, R. R. Birge, E. Kaplan, J. R. Tallent, *Nature* **1993**, *366*, 64–66.
[7] P. Ala-Laurila, K. Donner, A. Koskelainen, *Biophys. J.* **2004**, *86*, 3653–3662.
[8] D. G. Luo, W. W. S. Yue, P. Ala-Laurila, K. W. Yau, *Science* **2011**, *332*, 1307–1312.
[9] S. Gozem, I. Schapiro, N. Ferre, M. Olivucci, *Science* **2012**, *337*, 1225–1228.
[10] Y. Guo, S. Sekharan, J. Liu, V. S. Batista, J. C. Tully, E. C. Y. Yan, *Proc. Natl. Acad. Sci. USA* **2014**, *111*, 10438–10443.
[11] J. Rajput, D. B. Rahbek, L. H. Andersen, A. Hirshfeld, M. Sheves, P. Altoe, G. Orlandi, M. Garavelli, *Angew. Chem. Int. Ed.* **2010**, *49*, 1790–1793; *Angew. Chem.* **2010**, *122*, 1834–1837.
[12] N. J. A. Coughlan, K. J. Catani, B. D. Adamson, U. Wille, E. J. Bieske, *J. Chem. Phys.* **2014**, *140*, 164307.
[13] G. A. Eiceman, Z. Karpas, *Ion Mobility Spectrometry*, CRC, Boca Raton, FL, **2005**.
[14] S. L. Koeniger, S. I. Merenbloom, S. J. Valentine, M. F. Jarrold, H. R. Udseth, R. D. Smith, D. E. Clemmer, *Anal. Chem.* **2006**, *78*, 4161–4174.
[15] N. A. Pierson, L. Chen, D. H. Russell, D. E. Clemmer, *J. Am. Chem. Soc.* **2013**, *135*, 3186–3192.
[16] N. A. Pierson, S. J. Valentine, D. Clemmer, *J. Phys. Chem. A J. Phys. Chem. B J. Phys. Chem. B.* **2010**, *114*, 7777–7783.
[17] N. A. Pierson, S. J. Valentine, D. Clemmer, *Int. J. Mass. Spectrom.* **2014**, DOI: 10.1016/j.ijms.2014.07.012.
[18] M. F. Mesleh, J. M. Hunter, A. A. Shvartsburg, G. C. Schatz, M. F. Jarrold, *J. Phys. Chem.* **1997**, *100*, 16082–16086.
[19] A. A. Shvartsburg, M. F. Jarrold, *Chem. Phys. Lett.* **1996**, *261*, 86–91.
[20] Y. Toker, D. B. Rahbek, H. V. Kiefer, J. Rajput, R. Antoine, P. Dugourd, S. B. Nielsen, A. V. Bochenkova, L. H. Andersen, *Phys. Chem. Chem. Phys.* **2013**, *15*, 19566–19569.
[21] N. J. A. Coughlan, B. D. Adamson, K. J. Catani, U. Wille, E. J. Bieske, *J. Phys. Chem. Lett.* **2014**, *5*, 3195–3199.

Received: December 10, 2014
Revised: January 25, 2015
Published online: March 10, 2015

  